*Romanian Journal of Mechanics*
*Volume 2, Issue 1/2017, pp 14-28*, ISSN 2537 - 5229, *rjm.journals.srmta.ro*

# MECHANICAL BEHAVIOR OF FIBROUS MATERIALS WITH APPLICATION TO CONNECTIVE TISSUE

Catalin PICU, Mohammad ISLAM

Department of Mechanical, Aerospace and Nuclear Engineering, Rensselaer Polytechnic Institute, Troy, NY 12180
Corresponding author: Catalin PICU, E-mail: cpicu@scorec.rpi.edu

**Abstract** A review of the generic mechanical behaviour of random networks of filaments subjected to tension and compression is presented in this article. The system is athermal, in the sense that thermal fluctuations prevalent on the nanoscale have no effect on the mechanics of these fibers. The fibers are connected at cross-linking sites and behave as beams with axial, bending and torsional stiffness. Transient contacts between filaments are important primarily in compression. The stress-strain curve has three regimes in both tension and compression. The first regime is linear elastic, with modulus identical in tension and compression. The second regime is defined by exponential stiffening in tension and is associated with the non-affine convection of filaments. In compression, the stress-strain curve softens in the second regime and a plateau appears during which the fibers align in the plane perpendicular to the compression direction. The third regime corresponds to strong stiffening in both tension and compression. The cause of stiffening in tension is the formation of a load-bearing structure of fibers aligned in the tensile direction, while in compression, stiffening is associated with the formation of a large number of contacts between fibers. In both tension and compression, a very large Poisson effect is observed. These results are compared with the behavior of collagenous connective tissue and important similarities are observed. It is concluded that the type of models presented here are adequate for the representation of tissue mechanics.

*Key words*: Fiber networks, biological tissue, hyperelasticity, Poisson effect.

## 1. INTRODUCTION

Many of the materials in the living and non-living worlds are fibrilar, i.e. are either composed exclusively from closely interacting filaments or contain fibers embedded in a fluid or solid matrix. A common example is rubber, which is a cross-linked molecular network [1]. Gels are also molecular networks which are swollen by the absorption of water. Polymeric fibers with diameters on the order of several microns are used in a variety of consumer products. Nonwovens are made from fibers with high aspect ratio which are not bonded to each other, but entangle and interact frictionally [2]. Nonwovens are used for thermal insulation (e.g. fiber glass and felt), filtration and sound insulation. They are also used for liquid absorption in hygiene products. Fibers in nonwovens can be bonded by a variety of means, with the bonds being of the size of the fiber diameter or much larger entities which connect many fibers. Bonded polymeric fiber mats of this type are used in common and special clothing, consumer products, and in packaging.

A classical example of a fibrous material is paper, which is made from cellulose fibers with ribbon-like cross-section, held together by H-bonding [3]. Common paper contains cellulose filaments, while special papers may contain additives, such as a polymeric binder, which play the role of a matrix.

Most biological materials are made from filaments of various types and dimensions. The cytoskeleton of eukaryotic cells is a set of interpenetrating semi-flexible macromolecular (protein) networks which provide the structural integrity of the cell, host the cellular organelle and perform important functions in cellular division, migration and chemo-mechanical transduction [4]. The cytoskeleton mechanics is a subject of intense research today driven by the desire to gain control of the bio-chemical activity of the cell.

Connective tissue, in general, is a collagen network saturated with water and hosting other large-molecular entities with physiological role, such as proteoglycans (PG). The PG insure network swelling and prevent excessive compaction of the tissue under compression even when part of the water is expelled [5, 6]. Cartilage is a common example of connective tissue. It is composed from collagen fibrils with preferential alignment at the surface of the tissue (parallel to the surface) and at the bone interface (perpendicular to the interface), while the core of the tissue has random collage orientation [7]. Cartilage reduces the friction and wear during locomotion, therefore mitigating very large forces over a large number of loading cycles. Ligaments are also made primarily from collagen. In this type of tissue, it is common to observe preferentially oriented fibers, some being actually fiber bundles, which may cross the entire structure connecting the opposing bone surfaces [8]. Ligaments play an obviously central mechanical role in the osteo-articular system, but are also thought to act as sensing organs. Sparse innervation in ligaments makes possible sensing overloads, information which is then used as motion control input to the brain.

Blood vessels have a complex multi-layer structure, with the mechanical function being performed primarily by a composite network of collagen and elastin [9]. The elastin component provides almost constant stiffness over a broad range of strains. Collagen forms networks that exhibit strong strain stiffening. These have small stiffness at small strains, but stiffen up rapidly once the strain becomes larger than 5-10%. Therefore, the elastin component provides the main contribution to stiffness at small strains, while the collagen component takes over at larger strains. This allows the blood vessel diameter to increase at essentially constant stiffness, but prevents burst due to the strong stiffening of the collagen network.

Various membranes in the body are composed form collagen and elastin. Examples include basal membranes and the fetal membrane [10, 11]. These are quasi-two-dimensional networks which are quite stiff and tough in the in-plane direction, but fully flexible in the out-of-plane direction. Their mechanical function is essential in physiology.

This brief review presents the key aspects of the mechanical behavior of networks of athermal filaments and compares the results with experimental observations made on tissue and artificial collagen constructs. The linear and non-linear elastic components of the behavior are discussed in compression and tension. The structures of interest are not embedded in a matrix and are considered not to embed other entities (e.g. PG in cartilage, or cellular organelle in the cytoskeleton). Our data as well as data from the literature indicate that this type of models is adequate for representing connective tissue mechanics. This insight also applies to non-biological networks such as those described above, which are important in engineering.

## 2. MATERIAL STRUCTURE AND MODEL DEFINITION

Fiber networks are assemblies of filaments that fill the space at very small volume fractions. The characteristic lengths of such structures are the fiber diameter, $d$ (if fibers have circular sections), and the inverse of the filament density, $\rho$ (defined as the total length of filament per unit volume), which is proportional to the mean length of a segment between two cross-links, $l_c$. The aspect ratio of a filament, $l_c / d$, is usually larger than 10 and can be very large in sparsely cross-linked networks where $l_c$ is large. Due to this large difference between $d$ and $l_c$, the overall density of the material is low.

In collagenous networks the diameter of a collagen fibril is approximately 100 nm, but multiple fibrils may bundle in fibers of tens of microns diameter [12]. Bundling is promoted by pH variations and, in the case of artificial constructs, by polymerization at temperatures lower than the body temperature [13]. Cross-linking of two collagen fibrils is thought to be mediated by PG. The density of cross-liking is not easily measurable, so $l_c$ for networks made from the thinnest, unbundled filaments is poorly defined. However, data for collagen constructs are available, with $l_c$ usually cited in the range of 2-10 μm [14, 15].

Fibers may be straight between cross-links, or may be wavy. The tortuosity parameter is defined as the ratio between the physical filament length between two cross-link points and its end-to-end distance. In collagen networks, tortuosity is reported to range between 1.1. and 1.4 [14].

In some structures, the network is aligned in the unloaded state. These cases are of less importance here, as the focus is on understanding the mechanics of random isotropic networks, without the added complexity introduced by preferential alignment.

The nature of the cross-links is of importance [16]. These can be classified based on their mechanical function in pin joints, rotating pins and welded joints. Pin joints transfer forces between fibers, but not moments. Rotating pins transfer moments only along given fiber, but not between fibers bonded at the respective cross-link. Welded joints transmit both moments and force, along given filament and between filaments. The nature of the cross-links in biological networks depends on the type of entity considered. The interaction of two non-bundled collagen fibers resembles the rotating pin situation. However, a welded joint is more appropriate for the representation of a collagen bundle that splits into to sub-bundles or fibrils.

The degree of connectivity at network nodes is also of importance [16, 17, 18]. The connectivity, *z*, is defined as the number of network segments merging into given node. This parameter is central for network stability. The Maxwell criterion for a structure of trusses indicates that *z* must be larger than 2D, where D is the dimensionality of the space in which the network is defined, for the structure to be mechanically stable. In three dimensions the critical *z* is 6. However, most networks in nature are less connected, with *z* between 3 and 4. Therefore, these are sub-isostatic and have no stiffness in the initial configuration. Stretching leads to fiber alignment and the network acquires stiffness at finite strains [18, 19].

Networks with *z* smaller than the critical value can be stabilized at infinitesimal strains in a number of ways. Even a small filament bending stiffness stabilizes the network at any *z* [16,18]. Self-equilibrating eigenstrains, which can be introduced in the network, for example, by inserting pre-strained filaments, have a similar stabilizing effect. Therefore, collagen structures with *z* in the vicinity of 3, are unconditionally stable in the undeformed configuration.

Network models with various architectures have been considered in the literature [19]. These include Delaunay networks, Voronoi networks, and Mikado networks in 3D [e.g. 21, 22, 23]. Delaunay and Voronoi networks are duals to each other. A Voronoi network is constructed from a Voronoi tessellation of the space in which the network is defined. The edges of the Voronoi cells are retained as fibers and vertices are the network nodes. The connectivity of Voronoi network is *z* = 4, hence these networks are stable only if filaments have non-zero bending stiffness. The connectivity can be reduced to smaller values by selective deletion of network links. A Delaunay network has much larger connectivity and may be stable even if all filaments transmit only axial forces (trusses). The Mikado network is generally defined in two dimensions and is obtained by depositing fibers of given length, $L_0$, with random orientations and random positions of their center of mass, until the desired density is reached [23, 24]. Cross-links are introduced at all or a subset of the filament crossing points. For an infinite network, the coordination number if *z* = 4. Mikado networks have been constructed in three dimensions as well [22], by defining filaments of given length and random orientation and then connecting them at sites where the smallest distance between fiber axes becomes smaller than an imposed threshold (e.g. 1-2 fiber diameters).

Multiple studies performed over the last 10 years indicated that the mechanical behavior of these networks is qualitatively similar and that one may reproduce features exhibited by another network through a simple change of parameters [18, 20]. Based on this observation, Voronoi networks are considered in this work.

Voronoi networks have only one parameter that controls the geometry – the density, $\rho$. Note that $\rho_v = \rho\frac{\pi d^2}{4}$ is the volume fraction of the network. We use here $\rho_v$ in place of $\rho$ since this quantity is non-dimensional and its physical significance is more obvious. The distribution of segment lengths is Poisson and is fully characterized by its mean, $l_c$ [25]: $l_c \sim 1/\rho$. Figure 1 shows a realization of a Voronoi network used in this study.

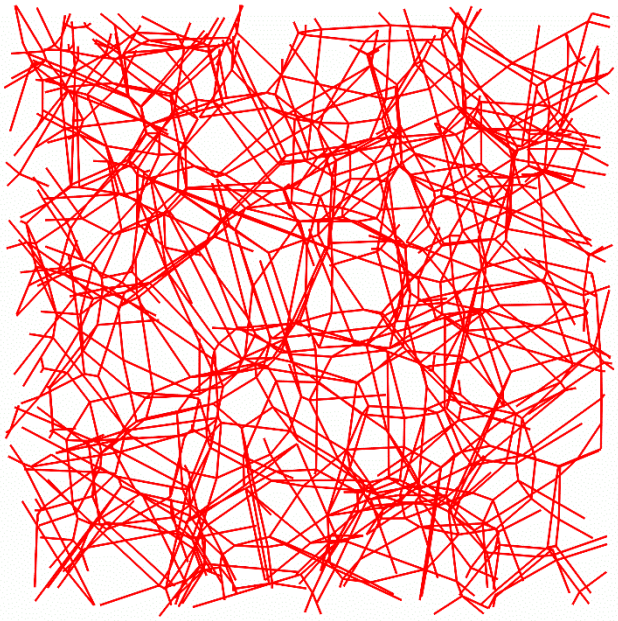

Fig. 1. Projection of a three dimensional Voronoi network in the undeformed state.

The relevant fiber properties are the Young's modulus of the fiber material, $E_f$, and the fiber diameter, $d$. These define the axial and bending rigidities, $E_f A$ and $E_f I$. The overall network behavior depends on $E_f A$ when the strain energy is stored primarily in the axial deformation mode of filaments and on $E_f I$ when the dominant deformation model is bending [16, 24, 26]. In general, three-dimensional networks of relatively low density are composed from filaments with large aspect ratio (large $l_c/d$) which deform predominantly in the bending mode. An alternate parameter frequently used in the literature is $l_b = \sqrt{E_f I/E_f A}$, which indicates the relative magnitude of the axial and bending rigidities [16, 24, 27]. $l_b$ has units of length and is equal to the fiber radius for filaments of circular section. The only relevant structural parameters for Voronoi networks composed from the same type of fiber (as opposed to situations in which multiple types of fibers are used and the network is "composite") are $\rho$ and $l_b$. In the current discussion, we keep $\rho$ and $l_b$ as parameters and analyze their effect on the network mechanical behavior.

The energy of the system is computed as the sum over all fibers of the stored energy in the axial, bending and shear mode

$$U = \frac{1}{2}\sum_{fibers}\int \kappa\left(\frac{\mathrm{d}\psi(s)}{\mathrm{d}s}\right)^2 + \eta\left(\frac{\mathrm{d}u(s)}{\mathrm{d}s}\right)^2 + \gamma\left(\frac{\mathrm{d}v(s)}{\mathrm{d}s} - \psi(s)\right)^2 \mathrm{d}s. \quad (1)$$

In this expression $v(s)$ represents the transverse displacement and $\frac{du(s)}{ds}$ is the axial strain at position $s$ along the fiber. The rotation of the fiber cross-section is $\frac{dv(s)}{ds}$, while $\psi(s)$ represents the

rotation of a plane which remains perpendicular to the neutral axis of the beam. Hence $\frac{dv(s)}{ds} - \psi(s)$ quantifies the shear deformation of the beam. This equation corresponds to the Timoshenko model of the beam. Note that the Euler-Bernoulli model is more often used for fibers [23]. In this case the energy of the system is computed with the same expression, without the third term under the integral. The two models give identical predictions for long, slender beams (beam length significantly larger than the cross-sectional dimension), while the Timoshenko model gives more accurate predictions for short beams [23]. It has been repeatedly reported that the energy stored in the torsion mode is negligible compared with the axial and bending energy [18]. In most studies, the shear term is also neglected, without significant changes of the behavior.

Here we are concerned with the response of the network to uniaxial tension/compression. Similar behavior has been observed in shear. Models similar to that shown in Fig. 1 are used and loaded uniaxially in displacement control. All degrees of freedom of nodes on the lateral faces of the model are left traction free. Displacements are applied (in the normal direction) on two opposing faces of the model. The other degrees of freedom (including the rotations) of the nodes for which displacements are specified are left traction free. The solution is found by using a general-purpose finite element solver (Abaqus).

## 3. GENERIC MECHANICAL BEHAVIOR OF RANDOM FIBER NETWORKS IN UNIAXIAL TENSION AND COMPRESSION

Fig. 2 shows a typical response of a random fiber network model subjected to uniaxial tension (nominal or first Piola-Kirchoff stress, $\sigma$, versus the stretch ratio in the loading direction, $\lambda$).

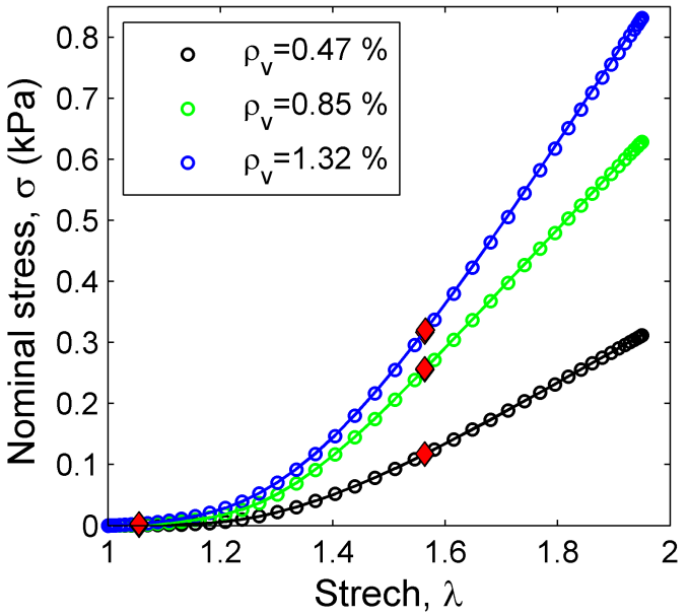


Fig. 2. First Piola-Kirchoff stress versus stretch response of Voronoi network of densities $\rho_v = 0.47$ %, 0.85 % and 1.32 %. The aspect ratio of fibers in these models is $l_c/d = 20$. The lines correspond to models in which fiber are not allowed to cross each other during deformation, while the symbols correspond to the opposite situation. The red symbols separate the three regimes described in text.

The axial and bending modulus of a fiber is defined by $E_f A$ and $E_f I$ respectively, where $E_f$ is Young's modulus of the fiber material, A is the cross-sectional area and $I$ is the moment of inertia of filaments. Young's modulus of a collagen fibril is reported in the broad range 30-800 MPa.

Here, we used 50 MPa and we assumed a circular cross-section with diameter 1 $\mu$m. The density of fiber bulk material is assumed to be 800 $\mathbf{kg/m^3}$.

Each of these curves exhibits three regimes: an initial linear regime in which the stress is proportional to the strain. The slope of these lines is the small strain modulus, $E_0$. Regime II corresponds to rapid, exponential stiffening. It begins at few percent strain and ends at approximately 50% strain. Regime III is again linear.

In the initial stage, the network deforms elastically, without significant distortion being observed. Deformations are mostly of the bending type, but geometric nonlinearity is minimal. Since the constitutive behavior of filaments is linear, the overall response of the network in Regime I is linear. As the network enters Regime II, fibers start to rotate towards the stretch direction. The large geometric nonlinearity leads to strong stiffening and a large Poisson effect. Fig. 3 shows a deformed configuration of the network represented in Fig. 1 (in red) together with the undeformed configuration (in black). The degree of filament orientation and the large associated Poisson contraction are obvious.

Regime III correspond to the formation of a strongly aligned structure of load bearing filaments [28]. A rather small fraction of the total number of filaments contribute. This structure is visible in Fig. 3. These models have been run under two conditions: allowing fibers to freely cross each-other (equivalent to the concept of “phantom chains” in polymer physics), and preventing them from crossing. The purpose of this analysis is to determine to what extent fiber-to-fiber contacts contribute to defining the stress-strain curve. The data in Fig. 2 indicate that for this type of network, contacts play no significant role in tension. These conclusions also hold for denser networks, where the probability to form contacts is larger.

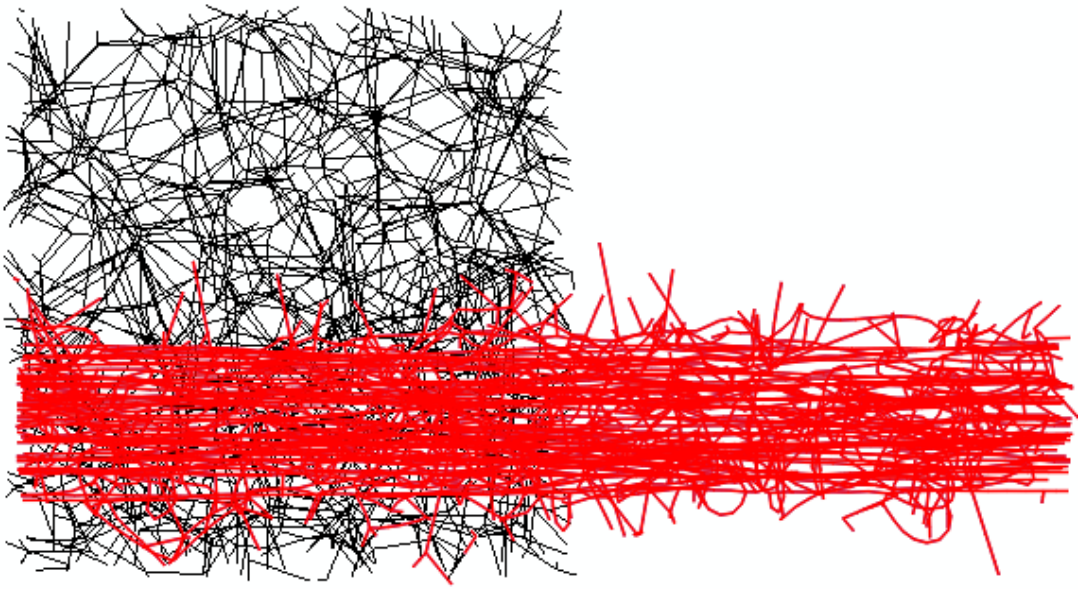

Fig. 3. Deformed network configuration (red) corresponding to an axial stretch of 1.92. The undeformed configuration is shown (black) for reference.

It is instructive to replot the data in Fig. 2 as the tangent stiffness versus stress, Fig. 4a. The three regimes become obvious in this representation. The linear behavior of Regime I leads to the plateau visible at small strains. The value of $E_0$ depends on the density [16, 24, 27]. The inset to Fig. 4b shows this dependence for the 3 systems shown here. It is seen that $E_0 \sim \rho_v^2$, as has been reported for other three-dimensional networks; this scaling is also observed in open cell foams [29]. However, the importance of Regime I is rather limited since it ends at rather small strains (Fig. 4b).

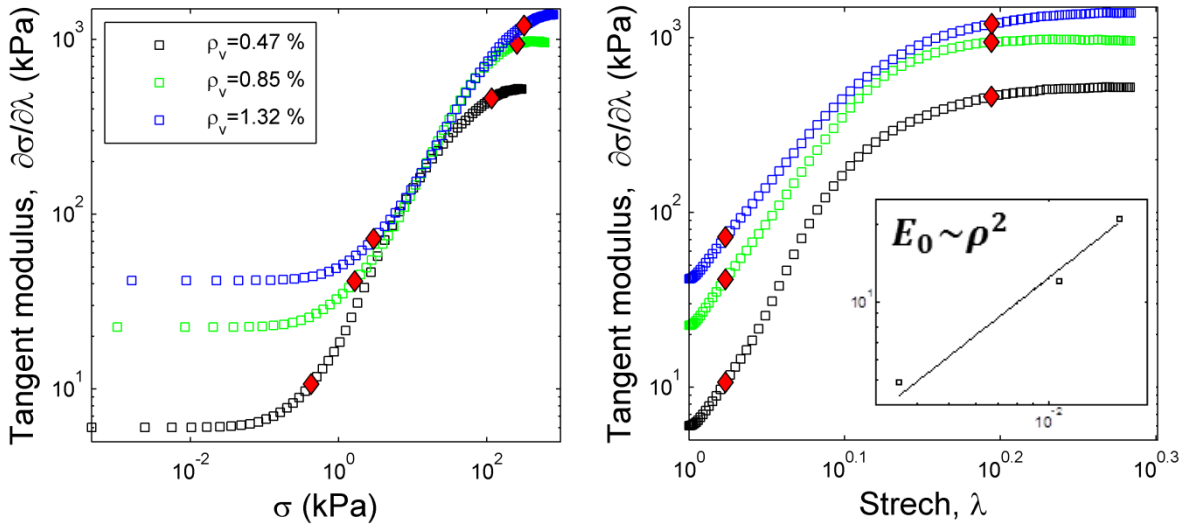


Fig. 4. Tangent modulus versus stress (a), and tangent modulus versus stretch (b) plots corresponding to the data in Fig. 2. The red symbols separate the three regimes of tensile behavior.

Regime II appears in the representation of Fig. 4a as a straight line of slope 1.

Therefore, the tangent modulus is proportional to the stress and hence the stress-strain curve is exponential. Curves corresponding to different densities and different $l_b$ parameters (not shown here) overlap in this regime. The regime covers a larger stress range for network of low density or/and low $l_b$ for which $E_0$ is small.

Note that since $\mathrm{d}\sigma/\mathrm{d}\varepsilon \sim \sigma$ in Regime II, and since Regime I is linear, all systems enter Regime II at the same strain, $\varepsilon_I$ (Fig. 4b). A similar statement can be made about the onset of Regime III, which occurs at a density and $l_b$-independent strain $\varepsilon_{II}$.

Since Regime III is linear, it appears in Fig. 4a as a horizontal line. All curves eventually reach this regime at large values of stress and strain. In physical networks, network damage may initiate way before reaching Regime III and this additional complexity changes the shape of the stress-stretch curve.

Further insight can be obtained by evaluating the partition of energy in the model throughout the deformation history. This is performed by post-processing the data obtained from the simulation. Fig. 5 shows the energy partition for the network of density $\rho_v = 0.85\%$ and $l_c/d = 10.5$.

The system stores energy mostly in the axial and bending modes. The contribution of the shear and torsion modes is small and essentially negligible for all these networks. In Regime I and for the most part of Regime II the bending mode dominates.

As the strain increases, the axial mode becomes more important and eventually becomes dominant in the second part of Regime II and in Regime III. This agrees with the qualitative understanding obtained from Figs. 2 and 4, and supports the direct observation of the formation of a strongly aligned fiber structure at large enough deformations. Therefore, a transition is observed from a bending-dominated behavior to a stretching-dominated one as strain increases.

The strain at which the curves corresponding to the bending and axial energies cross shifts to larger strains as the network density increases.

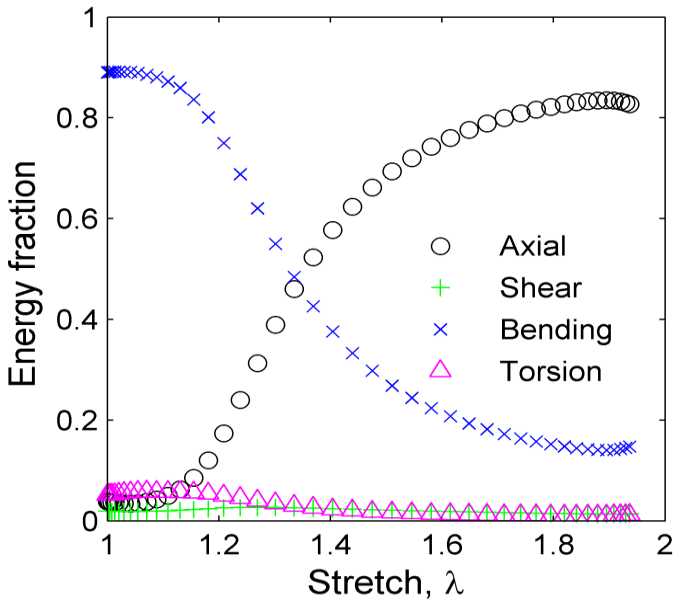


Fig. 5. Strain energy partition during uniaxial tension of the network with $\rho_v = 0.85\ \%$ and $l_c/d = 10.5$.

The degree of fiber orientation is quantified using the second Legendre polynomial based on the 11 entries of the orientation tensor. Specifically, we compute

$$P_2 = \frac{1}{2}(\langle cos^2\theta \rangle - 1), \tag{2}$$

where $\theta$ is the angle made by the end-to-end vector of a filament and the loading direction and $\langle\ \ \rangle$ indicates the ensemble average over the population of filaments. $P_2$ is zero if fibers are randomly oriented, 1 for perfect alignment in the stretch direction and -0.5 for perfect alignment in the plane perpendicular to the loading direction.

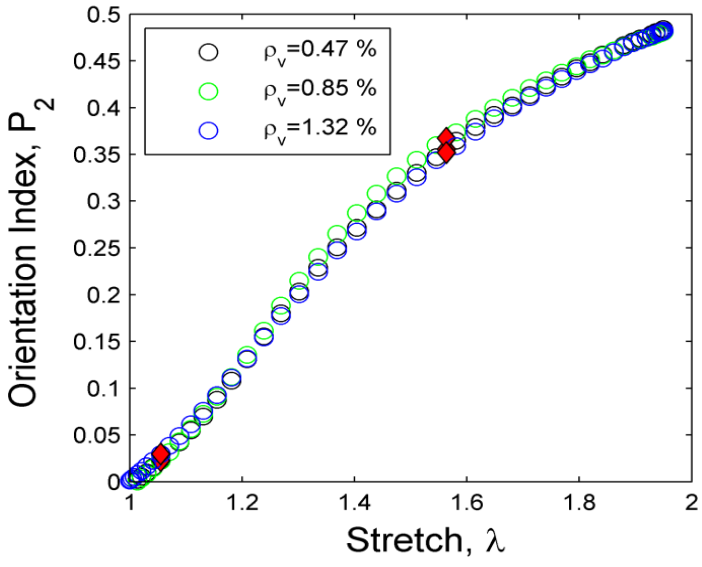


Fig. 6. Variation of the fiber orientation index $P_2$ during tensile deformation.

Fig. 6 shows the variation of $P_2$ with strain for the three systems of Figs. 2 and 4. It is seen that $P_2$ is approximately linear with the stretch up to approximately the transition from bending to axial dominated deformation (Fig. 5). The rate of orientation decreases at larger strains and, in particular, in Regime III. At very small strains, in Regime I, $P_2$ increases sub-linearly with strain since no

significant fiber convection is observed in this regime.

The pronounced convection of filaments leads to strong Poisson contraction. The effect is identical in the two directions perpendicular to the loading axis since the model is statistically isotropic in that plane. The initial Poisson ratio is initially approximately 0.3, but increases rapidly in Regime II. This is shown in Fig. 7. The figure shows the incremental Poisson ratio

$$\nu_i = -\frac{d\varepsilon_\perp}{d\varepsilon_\parallel} = -\frac{\lambda_\parallel}{\lambda_\perp}\frac{d\lambda_\perp}{d\lambda_\parallel} = -\frac{d\ln\lambda_\perp}{d\ln\lambda_\parallel}, \tag{3}$$

where $\lambda_\perp$ and $\lambda_\parallel$ are the stretch ratios in the direction perpendicular and parallel to the loading direction, respectively.

Further lateral contraction is limited in Regime III, and this is in agreement with the leveling trend of $P_2$ observed in Regime III in Fig. 6.

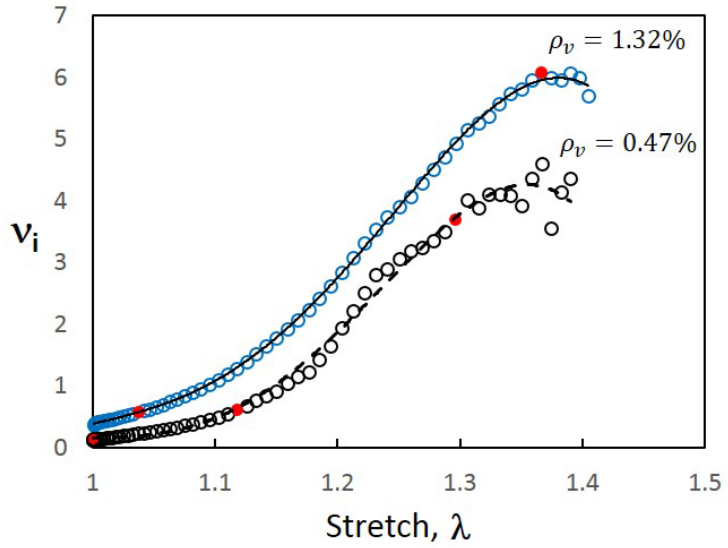


Fig. 7. Variation of the effective, incremental Poisson ratio, $\nu_i$ (eq. 3), with the stretch $\lambda = \lambda_\parallel$ during uniaxial tension.

A similar analysis performed in uniaxial compression reveals additional physics. The stress-strain curve is quite different from that of Fig. 2. Fig. 8a shows such curves for the three systems discussed so far ($\rho_v = 0.47,\ 0.85$ and 1.32, and $l_c/d = 10$). Once again, three regimes appear.

Regime I is linear elastic, of stiffness comparable with that measured in tension, $E_0$.

The small strain tensile stiffness is identical in tension and compression as long as no major filament rearrangement takes place and the constitutive behavior of filaments is identical in tension and compression. Note that even with crimped fibers, i.e. with filaments which are not straight in the initial configuration, the small strain modulus of the network would be identical in tension and compression. Regime I ends at a strain $\varepsilon_I$ which is close to, but slightly larger then, the upper limit of Regime I measured in tension.

Strong softening is observed once the strain becomes larger than $\varepsilon_I$ and Regime II begins. This leads to a quasi-plateau in the stress-strain curve and occurrence of localized collapse of the network. This feature is also observed in cellular materials, where the occurrence of the plateau indicates the formation of a major localization band which then advances along the gauge of the sample in the direction of the applied load [29].

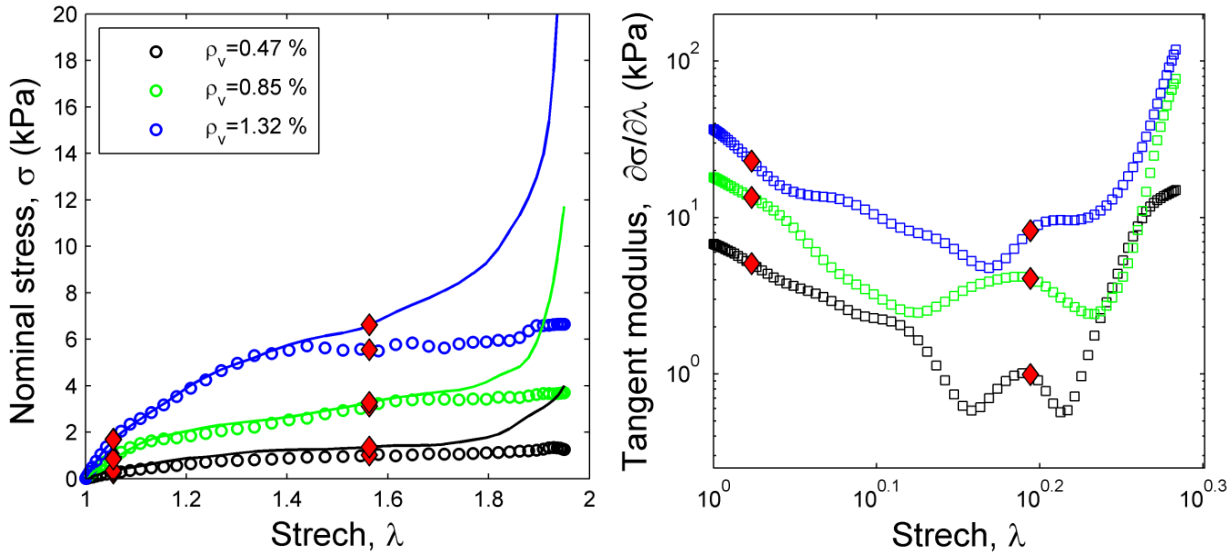


Fig. 8. (a) First Piola-Kirchoff stress versus stretch curves in compression for network of volume fractions $\rho_v = 0.47$ %, 0.85 % and 1.32 %. The aspect ratio of fibers in these models is $l_c/d = 10$. The lines correspond to models in which fiber are not allowed to cross during deformation, while the symbols correspond to phantom fibers. (b) shows the data in (a) replotted as tangent stiffness versus strain. The red symbols separate the regimes discussed in text.

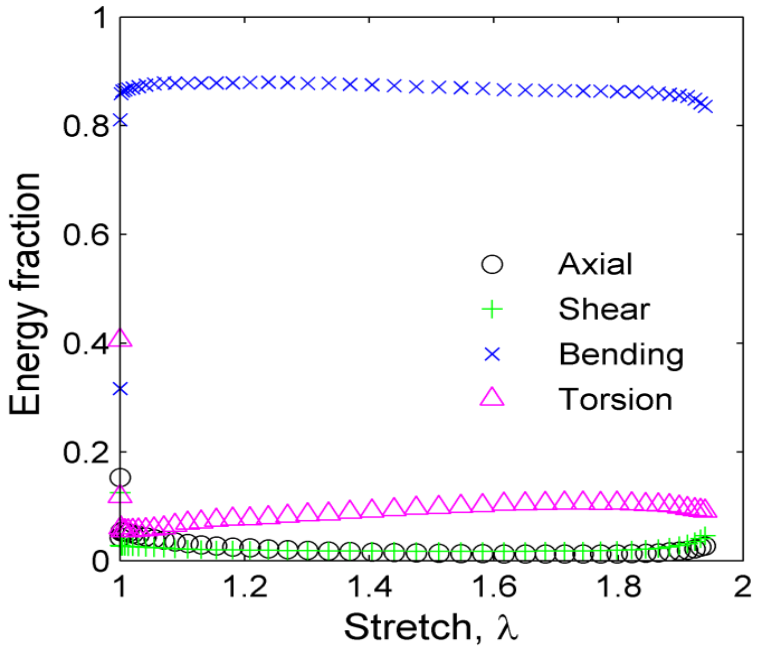


Fig. 9. Energy partition during uniaxial compression of the network with $\rho_v = 0.85\%$ and $l_c/d = 10$.

The sample deforms at almost constant stress, i.e. corresponding to the stress required to produce a localization band. In these networks, the behavior is slightly different due to the randomness of the structure. The plateau is not exactly flat (some small strain hardening is observed) and no advancing localization band can be observed in the sample. Rather, strain localization occurs more randomly, and apparently in an uncorrelated manner, over relatively small sub-domains of the sample.

A feature quite different from what is observed in tension is the contribution of fiber-fiber contacts to the overall behavior. Comparing the curves shown with continuous line with those shown

with symbols (Fig. 8a), it results that contacts lead to larger stresses in the plateau region.

In addition, in the absence of contacts there is no Regime III. Accounting for them leads to strong stiffening at very large compressive strains when the structure is essentially fully compacted (Regime III).

The energy partition is also quite different from the situation shown in Fig. 5. In these networks, the main contribution to the total energy is still associated with the bending mode, but no transition from an initial bending-dominated to an axial-dominated behavior at larger strains is observed, Fig. 9. The energy is stored primarily in the bending mode throughout the loading history. This is expected since in compression most fibers assume highly bent configurations for which the largest part of the strain energy is stored in the bending mode.

The fiber orientation is quantified with the same parameter used to analyze the tensile behavior, eq. (4), Fig. 10. $P_2$ takes negative values since filaments align preferentially in the plane perpendicular to the compression axis. In Regime I the orientation index increases in a manner resembling the tensile Regime I. During the plateau of Regime II, $P_2$ decreases slower with strain, while in Regime III filament orientation becomes more pronounced.

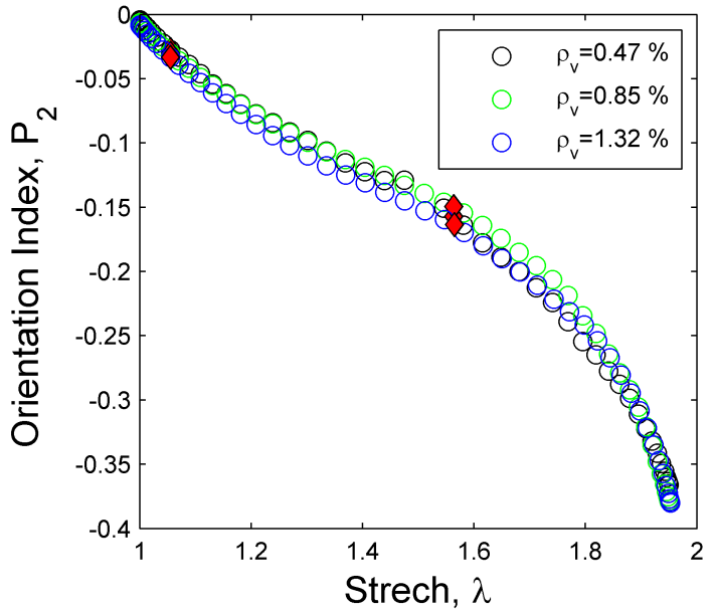


cross

Fig. 10**.** Variation of the fiber orientation index $P_2$ during compressive deformation.

The mechanical behavior presented here for tension and compression is also observed in networks with other architecture, e.g. Delaunay and Mikado networks, in both two and three dimensions [30].

Numerical values of various parameters describing the stress-strain or $P_2$ vs. strain curves depend on the network architecture, density or filament aspect ratio, but the central features outlined above are largely common to all networks. Due to this high level of generality, most of these features are observed in physical networks, including biological fibrous materials. The data discussed in this section is compared with experimental results for connective tissue in the next section.

## 4. COMPARISON WITH MECHANICAL BEHAVIOR OF TISSUE

In this section we present selected data from the literature representing the mechanical behavior of two types of tissue: rabbit renal tubules [10] and mouse dermis [31], which is the component of the skin that provides stiffness and strength to the tissue. Due to the nature of these

samples, tests were performed only in tension.

In both structures, the main contributor to the mechanical function is a network of collagen of small thickness. The properties of individual collagen fibrils have been measured by several authors (see [12] for a review) who worked with fibrils of different dimensions, ranging from hundreds of nm to tens of microns. In connective tissue such as in tendon, collagen fibrils assemble in fibers which then assemble in fascicles. In membranes, collagen organization in larger filaments remains limited. Therefore, we consider that the relevant fibril diameter for the tissues discussed is in the range 0.1 and 1 μm [12, 15, 21].

Such filaments exhibit an almost linear stress-strain curve up to a strain of about 20%, with strong stiffening beyond 30% strain. The stiffness is in the range 100 MPa to 1 GPa [12].

The degree of cross-linking and the nature of the cross-links are not entirely known. Likewise, the collagen density can vary in a broad range and is generally not reported in tissue level studies. Artificial networks of collagen (collagen constructs) generally have collagen concentration in the range 0.5 to 4 mg/ml.

Figure 11(a) shows the first Piola-Kirchoff stress-stretch curves for rabbit renal tubules and for mouse dermis [10,31]. The renal tubules were subjected to controlled internal pressure and the diameter was measured during inflation. The dermis samples were obtained by separating it from a skin sample and were loaded in uniaxial tension. In both cases there is some uncertainty with respect to the reference, zero stress state. This originates from the fact that tissue deforms at very small stresses which may not be measurable in an ex-vivo experiment. Therefore, most researchers report as the reference point the state of the sample at which the signal from the force transducer emerges from the noise.

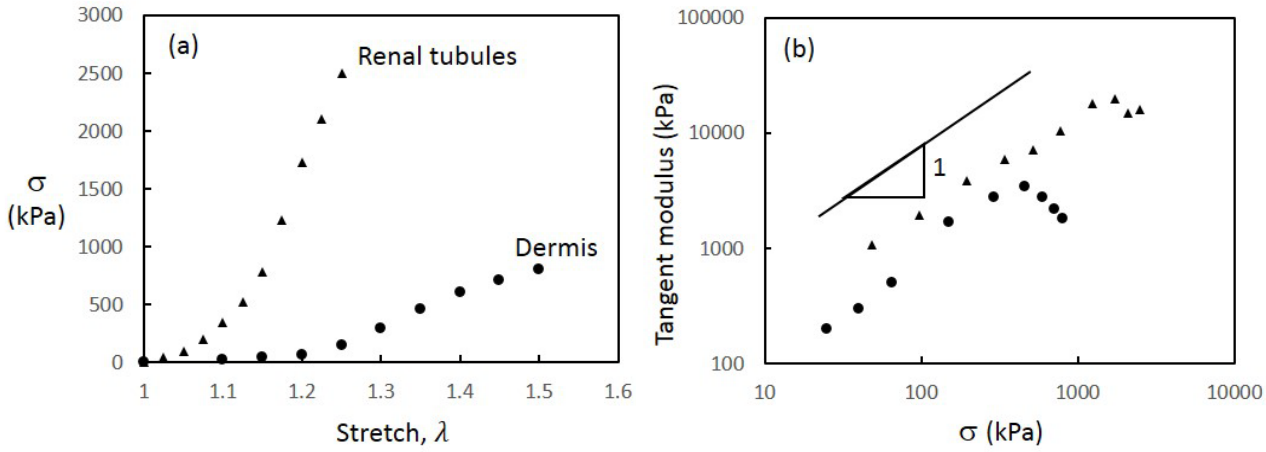


Fig. 11. (a) First Piola-Kirchoff stress versus stretch curves for rabbit renal tubules (triangles, adapted from [10]) and mouse dermis (circles, adapted from [31]); (b) Data in (a) re-plotted as tangent stiffness versus stress.

The two curves exhibit typical response for tissue composed from three regimes: a “toe” regime in which the stress is very small and definite statements about the nature of the stress-stretch curve cannot be made, a “heel” region in which the stress-stretch curve is exponential, followed by a linear regime. These correspond closely to the three regimes discussed in the previous section for random fiber networks. In both cases, a final regime in which the slope of the stress-stretch curve decreases is observed at larger strains. This regime is usually associated with damage accumulation.

The response of the dermis is significantly softer than that of the renal tubules. However, the main features of the stress-stretch curve are present. These are evidenced in Fig. 11(b) where the data in Fig. 11(a) is plotted in log-log coordinates as tangent stiffness versus stress.

Regime 1 of the network is not visible probably because the stress was below the resolution of the force measurement and/or because it was eliminated during data processing. However, Regime

II defined by a straight line of slope 1 in this type of plot is clearly visible for both tissues. Furthermore, both curves bend over to a short plateau, which is indicative of Regime III of the network, before the slope becomes negative, which indicates damage accumulation. Clearly, this last feature which was absent in the discussion about the fiber networks can be reproduced if damage accumulation is allowed to occur in models.

This discussion indicates that fiber network models are able to reproduce the key features observed in tissue mechanics. This observation is not singular or specific to these two types of tissues discussed here, rather, it was made previously for other tissues, including human samples.

While the behavior analyzed so far can be reproduced by constitutive equations of the hyperelastic type, the very large Poisson ratio (most of the time larger than 0.5) exhibited by fiber networks (Fig. 7) poses significant problems. It is of interest to clarify whether such large Poisson effects are observed in tissue.

Figure 12 shows the variation of the incremental Poisson ratio (defined by eq. (3)) for the dermis [31]. The Poisson effect was not measured in the experiments performed on renal tubules in [10]. The value of $\lambda_{\parallel} \equiv \lambda$ is controlled, while $\lambda_{\perp}$ is measured in the plane of the sample. The thickness of the sample being small, evaluating the stretch in the third direction is not possible. In the initial phase of deformation, the effective, incremental Poisson ratio is negative, likely due to water drainage. A strong Poisson effect is observed at larger strains. As in the case of the model networks, this effect is associated with strong filament alignment in the loading direction and is mostly a kinematic effect. Similar very large values of the Poisson ratio have been observed in most connective tissue, in the human amnion and in artificial collagen gels [11, 32].

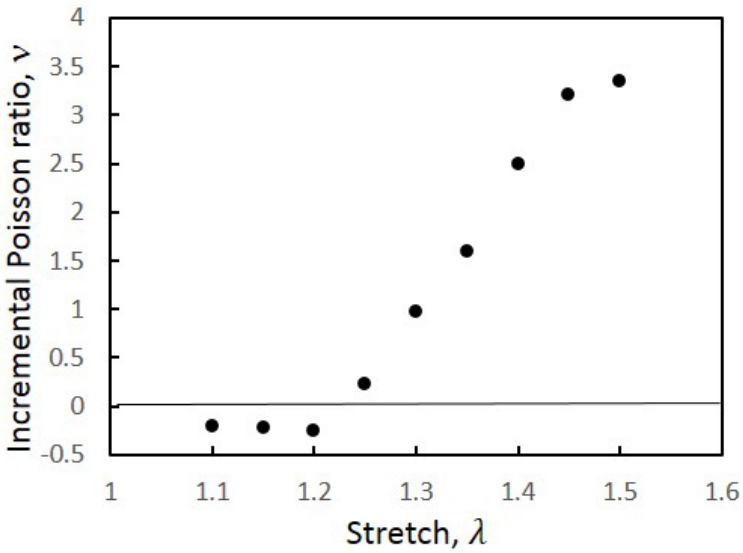


Fig. 12. Incremental Poisson ratio (eq. (3)) measured for the mouse dermis samples. Adapted from [31].

## 5. CONCLUSIONS

This article presents a review of the main features of the mechanical behavior of random networks. These exhibits non-linear behavior with the main source of non-linearity being geometric, i.e. associated with the convection of filaments in the principal loading direction. Filament constitutive non-linearity plays a secondary role, primarily because individual filaments are loaded to only a fraction of the strain applied to the network scale.

Fiber convection leads to exponential stress-strain curves which are broadly observed in various types of network-based materials such as tissue. Network models also indicate that the strain energy is stored primarily in the bending mode of filaments, but at large strains a transition to axial energy storage is observed. Filament kinematics is directly quantified by monitoring the

orientation distribution. This is done in experiments in-situ, during deformation, via optical means. The strong filament orientation leads to very large Poisson effects which are observed in models, in most connective tissue and in non-biological network-based materials.

This analysis demonstrates that random fiber network models can be used to predict the mechanics of tissue, scaffolds for tissue growth and tissue analogs. They promise to play an important role in the design of future biomedical materials.

**Acknowledgment**: This work was supported in part by the US National Science Foundation through grant CMMI-1634328 and CMMI-1362234.

## REFERENCES

1. TRELOAR, R.L.G., *The physics of rubber elasticity*, Clarendon Press, Oxford, 1975.
2. HORROCKS, A.R., ANAND, S.C., Eds., Handbook of technical textiles, CRC Press, Boca Raton, FL, 2000.
3. GELLERSTEDT, M.Ek.G., HENRIKSSON, G., *Paper products physics and technology*, W. de Gruyter, Netherlands, 2009.
4. MOFRAD, M.R.K., KAMM, R.D., *Cytoskeletal mechanics: models and measurements*, Cambridge Univ. Press, Cambridge, UK, 2006.
5. FUNG, Y.C., *Biomechanics: mechanical properties of living tissue*, Springer-Verlag, New York, 1993.
6. GRODZINSKY, L.Ng.A.J., PATWARI, P., SANDY, J., PLAAS, A., ORTIZ, C., J. Struct. Biol., 143 242, 2003.
7. MANSFIELD, J.C. WINLOVE, C.P., MOGER, J., MATCHER, S.J., J. Biomed. Optics 13, 044020, 2008.
8. ZHANG, S., BASSETT, D.S., WINKELSTEIN, B.A., J. R. Soc. Interface 13, 20150883, 2016.
9. HOLZAPFEL, G.A., OGDEN, R.W., Eds., *Mechanics of biological tissue*, Springer-Verlag, Berlin, 2006.
10. WELLING, L.W., ZUPKA, M.T., WELLING, D.J., Physiology 10, 30, 1995.
11. MAURI, A., EHRET, A.E., PERRINI, M., MAAKE, C., KOLBLE, N.O., EHRBAR, M., OYEN, M.L., MAZZA, E., J. Biomech. 48, 1606, 2015.
12. SHERMAN, V.R., YANG, W., MEYERS, M.A., J. Mech. Beh. Biomed. Mater. 52, 22, 2015.
13. YANG, Y.L., LEONE, L.M., KAUFMAN, L.J., Biophys. J. 97, 2051, 2009.
14. LAI, V.K., FREY, C.R., KERANDI, A.M., LAKE, S.P., TRANQUILLO, R.T., BAROCAS, V.H., Acta Biomater. 8, 4031, 2012.
15. LINDSTROM, S.B., KULACHENKO, A., JAWERTH, L.M., VADER, D.A., Soft Matter 9, 7302, 2013.
16. PICU, R.C., Soft Matter 7, 6768, 2011.
17. SHARMA, A., LICUP, A.J., JANSEN, K.A., RENS, R., SHEINMAN, M., KOENDERINK, G.H., MacKINTOSH, F.C., Nature Phys. 12, 584, 2016.
18. BROEDERSZ, C.P. MacKINTOSH, F.C., Rev. Modern Phys. 86, 995, 2014.
19. WYART, M., LIANG, H., KABLA, A., MAHADEVAN, L., Phys. Rev. Lett. 101, 215501, 2008.
20. HEUSSINGER, C, FREY, E., Phys. Rev. E 75, 011917, 2007.
21. LAKE, S.P., HADI, M.F., LAI, V.K., BAROCAS, V.H., Annals Biomed. Eng. 40, 2111, 2012.
22. ONCK, P.R., KOEMAN, T., van DILLEN, T., van der GIESSEN, E., Phys. Rev. Lett. 95, 179102, 2005.

23. SHAHSAVARI, A., PICU, R.C., Phys. Rev. E 86, 011923, 2012.
24. HEAD, D. A., LEVINE, A. J., MacKINTOSH, F. C., Phys. Rev. Lett. 91, 108102, 2003.
25. KALLMES, O. CORTE, H., Tappi journal 43, 737, 1960.
26. HEUSSINGER, C. FREY, E., Phys. Rev. Lett. 97, 105501, 2006.
27. SHAHSAVARI, A.S., PICU, R.C., Phil. Mag. Lett. 93, 356, 2013.
28. ZAGAR, G., ONCK, P.R., van der GIESSEN, E., Biophys. J. 108, 1470, 2015.
29. GIBSON, L.J., ASHBY, M.F., *Cellular solids: Structure and properties*, Cambridge Univ. Press, Cambdridge, UK, 1999.
30. LICUP, A.J., MUNSTER, S., SHARMA, A., SHEINMAN, M., JAWERTH, L.M., FABRY, B., WEITZ, D.A., MacKINTOSH, F.C., Proc. Nat. Acad. Sci. 112, 9573, 2015.
31. BANCELIN, S., LYNCH, B., BONOD-BIDAUD, C., DUCOURTHIAL, G., PSILODIMITRAKOPOULOS, S., DOKLADAL, P., ALLAIN, J.M., SCHANNE-KLEIN, M.C., RUGGIERO, F., Scientific Reports 5, 17635, 2015.
32. VADER, D., KABLA, A., WEITZ, D., MAHADEVAN, L., PLoS One 4, e5902, 2009.

*Received February 5, 2017*